Annals of Clinical and Translational Neurology

RESEARCH ARTICLE OPEN ACCESS

Amygdala Neurodegeneration: A Key Driver of Visual Dysfunction in Parkinson's Disease

Asier Erramuzpe[1,2] | Ane Murueta-Goyena[3,4] | Antonio Jimenez-Marin[1] | Marian Acera[3] | Sara Teijeira-Portas[3] | Rocío Del Pino[3] | Tamara Fernández-Valle[3] | Ibai Diez[1,2] | Unai Sainz-Lugarezaresti[1] | Naroa Ibarretxe-Bilbao[5] | Unai Ayala[6] | Maitane Barrenechea[6] | Alberto Cabrera-Zubizarreta[7] | Jesús Cortés[1,2,8] | Juan Carlos Gómez-Esteban[3,4] | Iñigo Gabilondo[2,3]

[1]Computational Neuroimaging Group, Biobizkaia Health Research Institute, Barakaldo, Spain | [2]Bilbao, Spain | [3]Neurodegenerative Diseases Group, Biobizkaia Health Research Institute, Barakaldo, Bizkaia, Spain | [4]Department of Neurosciences, Faculty of Medicine and Nursery, University of the Basque Country (UPV/EHU), Leioa, Spain | [5]Department of Psychology, Faculty of Health Sciences, University of Deusto, Bilbao, Spain | [6]Biomedical Engineering Department, Faculty of Engineering, Mondragon University, Mondragon, Spain | [7]OSATEK Magnetic Resonance Imaging Unit, Galdakao Hospital, Galdakao, Spain | [8]Department of Cell Biology and Histology, University of the Basque Country (UPV/EHU), Leioa, Spain

Correspondence: Iñigo Gabilondo (igabilon@gmail.com)

Received: 23 September 2024 | **Revised:** 28 January 2025 | **Accepted:** 1 February 2025

Funding: This work was supported by Eusko Jaurlaritza, PRE_2019_1_0070, Ministry of Science, Innovation and Universities (MICIU) (Spain), RYC2022-035429-I Instituto de Salud Carlos III, JR15/00008, PI14/00679, PI16/00005, Ikerbasque, Basque Foundation for Science, Contracts for AE, JC and IG, Berrikuntza + Ikerketa + Osasuna Eusko Fundazioa, 2016111009, 2020333033, Michael J. Fox Foundation for Parkinson's Research, RRIA 2014 Program/grant ID: 10189.

Keywords: amygdala | brain MRI | neurodegeneration | retina | vision

ABSTRACT

Objective: Visual disability in Parkinson's disease (PD) is not fully explained by retinal neurodegeneration. We aimed to delineate the brain substrate of visual dysfunction in PD and its association with retinal thickness.

Methods: Forty-two PD patients and 29 controls underwent 3-Tesla MRI, retinal spectral-domain optical coherence tomography, and visual testing across four domains. Voxel-level associations between gray matter volume and visual outcomes were used to define a visual impairment region (*visualROI*). Functional connectivity of the *visualROI* with brain networks was analyzed. Covariance analysis of brain regions associated with retinal thinning (*retinalROI*) was conducted using hierarchical clustering to develop a model of retinal and brain neurodegeneration linked to disease progression.

Results: The amygdala was the primary component of the *visualROI*, comprising 32.3% and 14.6% of its left and right volumes. Functional connectivity analysis revealed significant disruptions between the *visualROI* and medial/lateral visual networks in PD. Covariance analysis identified three clusters within *retinalROI*: (1) the thalamic nucleus, (2) the amygdala and lateral/occipital visual regions, and (3) frontal regions, including the anterior cingulate cortex and frontal attention networks. Hierarchical clustering suggested a two-phase progression: early amygdala damage (Braak 1–3) disrupting visual network connections, followed by retinal and frontal atrophy (Braak 4–5) exacerbating visual dysfunction.

Interpretation: Our findings support a novel, amygdala-centric two-phase model of visual dysfunction in PD. Early amygdala degeneration disrupts visual pathways, while advanced-stage disconnection between the amygdala and frontal regions and retinal neurodegeneration contributes to further visual disability.

Abbreviations: FC, functional connectivity; GCIPL, ganglion cell-inner plexiform layer complex; GM, graymatter; LCVA, low contrast visual acuity; MRI, magnetic resonance imaging; OCT, optical coherence tomography; PD, Parkinson's disease; ROI, region of interest; VAPS, visual attention and processing speed; VCON, visual construction; VMEM, visual memory; VPER, visual perception.

1 | Introduction

Interest in visual research in Parkinson's disease (PD) has grown due to evidence suggesting that visual dysfunction is an early clinical feature [1, 2] and a predictive biomarker of cognitive deterioration [3, 4]. Research on visual dysfunction in PD dates back several decades, with early studies by Bodis-Wollner in the late 1970s demonstrating deficits in visual evoked potentials [5], highlighting the involvement of both retinal and cortical pathways in PD-related visual impairments. Since then, numerous studies have explored both basic and higher-order visual deficits in PD. Work by Cronin-Golomb and colleagues has extensively documented impairments in visuospatial function, mental rotation, facial recognition, and facial emotion processing [6–10]. Similarly, Harris, Lee, and Amick have provided evidence of deficits in contrast sensitivity, optic flow perception, biological motion detection, visual scanning, and bistable perception in PD [11–15]. Wagenaar and collaborators have further demonstrated impairments in navigation and spatial perception, linking these deficits to abnormal processing of optic flow stimuli [16–19]. Jaywant et al. have investigated the relationship between visual and motor symptoms, showing how disruptions in visual perception can contribute to gait disturbances and postural instability [20–25]. Collectively, these studies emphasize that visual dysfunction in PD extends beyond contrast sensitivity deficits and involves complex interactions between visuoperceptual, visuospatial, attentional, and cognitive domains.

The retina has been a primary focus of visual dysfunction studies in PD. It is now well established that in PD early on, even from pre-motor phases [26–28], neurodegeneration of inner retinal cells occurs, involving the amacrine dopaminergic cells and the retinal ganglion cells of the parafovea [26, 29–32]. Retinal abnormalities, confirmed through optical coherence tomography (OCT), correlate with visual deficits [28]. Dopamine deficits observed in retinal cells explain the partial reversibility of some symptoms, such as contrast sensitivity, with L-Dopa therapy in early stages [33]. However, visual disturbances in PD cannot be fully explained by retinal changes [28], suggesting that brain alterations also play a key role and could help better explain the early and persistent visual deficits in PD.

While primary visual cortex atrophy occurs in late stages [34, 35], early-stage patients show occipital lobe hypometabolism [36], blood hypoperfusion [37], and reduced N-acetylaspartate levels [38]. These changes are linked to increased risks of cognitive decline and dementia, possibly driven by altered functional connectivity (FC) of the occipital cortex with other brain regions affected early in PD [39], such as cortical and subcortical hubs participating in ventral or dorsal associative visual networks. Most previous brain imaging studies addressing visual abnormalities in PD have focused on visual hallucinations or cognitive impairment but only a few have specifically evaluated the relationship between visual impairment and structural and functional brain alterations [40–47]. However, variations in imaging analysis techniques, cognitive tests, and task designs have resulted in divergent results.

In this study, we evaluated idiopathic PD patients and controls by combining multidomain psychophysical visual tests, multimodal brain imaging, and retinal OCT to investigate the structural and functional alterations underlying visual dysfunction in PD. Through a novel methodological approach that integrates voxel-level association maps across four visual domains, we looked for the common neuroanatomical substrate of visual disability in PD, exploring its impact on brain FC and evaluating its relationship with retinal neurodegeneration and disease progression stages.

2 | Methods

2.1 | Study Design and Participants

We conducted a cross-sectional evaluation of 42 patients with idiopathic PD (iPD) and 29 controls, recruited from Cruces University Hospital. Patients met the UK Brain Bank criteria for PD diagnosis [48] and were assessed in on-medication condition. We excluded participants with neurological, ophthalmological or systemic diseases other than PD that could affect study outcomes, as described before [49]. Exclusions included neurological, ophthalmological, or systemic diseases potentially affecting outcomes, as well as genetic forms of PD identified through routine clinical testing (LRRK2, PARK2, SNCA mutations: genetic testing was performed in individuals with more than one first or second-degree relative affected by the disease or those under 50 years of age). Controls were excluded if they had more than one first-degree relative with PD or PD-like symptoms. The Basque Clinical Research Ethics Committee approved the protocol (ID: PI2014154).

2.2 | Demographical Features and PD-Related Variables

Age, sex, and years of education were recorded. For iPD patients, disease duration, Hoehn & Yahr Scale score, Unified Parkinson's Disease Rating Scale (UPDRS) score, and Levodopa equivalent daily dose (LEDD) were documented.

2.3 | Visual and Cognitive Outcome Assessment

Binocular high-contrast and low-contrast visual acuity (LCVA) was measured using ETDRS and Sloan 2.5% charts, respectively, at 4 m with best correction and recorded as the total number of correct letters. LCVA was chosen as a marker of primary visual function due to its strong correlation with retinal atrophy and cognitive impairment in PD [3, 4, 27]. General cognition was evaluated with the Montreal cognitive assessment (MoCA). Visual cognition was assessed through a neuropsychological battery grouped into three domains, as described previously [28]: (1) visual attention and processing speed (VAPS), including Salthouse Perceptual Comparison Test, Trail Making Test—part A, and Symbol Digit Modalities Test; (2) visual perception (VPER), including Picture Completion subtest of the Wechsler Adult Intelligence Scale IV, Benton Judgement of Line Orientation Test, and

Number Location and Cube Analysis tests of the Visual Object and Space Perception battery; (3) visual construction (VCON), consisting of Clock Drawing Test. Composite scores were calculated for LCVA, VAPS, VPER, and VCON. Visual hallucinations were screened using the North-East Visual Hallucinations Interview (NEVHI) [50].

2.4 | Retinal OCT Acquisition and Preprocessing

Macular volumetric images were obtained with a Spectralis spectral-domain OCT system (Heidelberg Engineering, Heidelberg, Germany). Images met OSCAR-IB quality criteria [51] and the built-in software segmented macular layers (HRA Spectralis Viewing Module version 6.0.9.0). The thickness of the parafoveal ganglion cell-inner plexiform layer complex (GCIPL) was analyzed, as it is the most affected measure in PD and strongly relates to visual outcomes [26, 28]. Measurements from both eyes were averaged, following APOSTEL guidelines [52].

2.5 | Brain Imaging Acquisition and Analyses

MRI was performed using a Philips 3-Tesla scanner with a 32-channel head coil, including T1-weighted and resting-state functional sequences. T1 images were processed with FSL's (version 6.0.1) voxel-based morphometry (VBM) protocol, including brain extraction, MNI152 registration, modulation, and smoothing. Functional images were preprocessed using the FC CONN (v18b) toolbox [53], with the default pipeline for volume-based analyses that included denoising and band-pass filtering [54]. Group comparisons accounted for head size using FSL-SIENAX (see Supporting Information for a full description of image acquisition parameters and preprocessing steps).

2.6 | Calculation of the *visualROI*

VBM was used to examine the relation between gray matter volume in specific areas of the brain and visual function in both iPD patients and healthy controls. We looked at the four different measures of visual function and controlled for factors like age and head size while analyzing the data separately for patients and controls. Threshold-Free Cluster Enhancement (TFCE) with 5000 iterations was used for multiple comparison correction. The four VBM corrected-maps were then intersected to detect common ROIs whose volume had a significant association with all the four visual outcomes, defining the so-called *visualROI*. The significance of the maps was adjusted to achieve a non-null intersection, that occurred at $q = 1 - p$ equal to 0.8, the smallest threshold that guaranteed a non-null intersection across all maps. The automated anatomical labeling atlas (AAL) was used to anatomically describe the *visualROI*.

2.7 | Functional Connectivity of the *visualROI* with Major Brain Networks

Seed-based FC analysis was performed using the *visualROI* as the seed. ROI-to-ROI analyses compared FC in iPD and controls, and the iPD<control contrast was conducted. The "CONN network cortical ROIs atlas" defined 31 ROIs grouped into 8 functional networks including the visual network, which is composed of 4 ROIs: medial visual (anatomically corresponding to cuneus, lingual, and fusiform gyrus), occipital visual (pericalcarine and lateral occipital cortex), left lateral visual, and right lateral visual (inferior temporal, middle temporal, superior temporal and supramarginal gyrus, and inferior parietal cortex) (see Supporting Information for a detailed description). Age was included as a confounding factor in the regression analyses. Connectivity circular graphs were created with false discovery rate (FDR) corrected $p < 0.05$ to binarize the 33×33 resulting resting-state FC matrices.

2.8 | Calculation of the *retinalROI* and Analysis of Retinal-Brain Neurodegeneration

VBM identified brain regions associated with GCIPL thickness (*retinalROI*) in iPD patients. The intersection of *retinalROI* and *visualROI* determined regions associated with both retinal thinning and visual dysfunction. Finally, with the aim of identifying models that better explain the relationship between neurodegeneration of the retina, amygdala, and brain, we analyzed the volumetric correlation of the different anatomical components of *retinalROI*. We extracted gray matter partial volume estimates from brain regions associated with parafoveal GCIPL thickness (*retinalROI*) and calculated the covariance between these regional volumes to identify clusters of regions exhibiting simultaneous atrophy, potentially indicative of distinct disease stages. Hierarchical clustering was used to define these clusters. We compared the identified clusters with Braak stages for alpha-synuclein pathology to determine which cluster/disease stage was most strongly associated with retinal volume loss.

2.9 | Statistical Analysis of Data

Analyses were performed in R (v3.6.1) and Python's statsmodels toolbox. Normality was assessed with the Shapiro-Wilks test. Continuous variables were compared using Mann–Whitney *U* or Kruskal–Wallis tests, with Dunn's post hoc test for multiple comparisons. Categorical variables were analyzed with Fisher's exact test. Correlations were evaluated with Spearman coefficients, and *p*-values were FDR-corrected ($p < 0.05$).

2.10 | Data Sharing

Datasets are not publicly available publicly due to patient privacy regulations but may be requested from the corresponding author upon reasonable request.

3 | Results

3.1 | Demographics and Clinical Characteristics of Study Population

Table 1 summarizes demographic and clinical characteristics of participants. No statistically significant differences were found in age or education years between iPD and controls,

TABLE 1 | Demographic and clinical characteristics of study participants.

	iPD	Controls	*p*
N	42	29	
Demographics			
Age (years)	60.3 (8.3)	59.8 (7.0)	0.781
Males, *n* (%)	28 (66.7)	12 (41.4)	0.035
Education, years	10.5 (4.2)	12.2 (4.2)	0.108
PD-related features			
Disease duration, years	6.1 (3.6)	—	—
Age at disease onset, years	54.2 (7.8)	—	—
LEDD, mg/day	595.6 (354.6)	—	—
UPDRS I	2.1 (1.7)	—	—
UPDRS II	11.3 (5.7)	—	—
UPDRS III	26.9 (11.3)	—	—
UPDRS IV	3.9 (3.5)	—	—
Hoehn & Yahr	2.0 (1.0 to 3.0)	—	—
Presence of visual hallucinations, *n* (%)	7 (16.7%)	—	—
Cognitive status			
MoCA total score	24.6 (3.1)	26.6 (3.2)	0.009
Visual outcomes			
High-contrast VA, no. of letters	59.2 (5.9)	61.6 (4.2)	0.061
Low-contrast VA, no. of letters (LCVA)	29.1 (10.8)	38.0 (6.2)	< 0.001
Visual attention and processing speed (VAPS)	−0.1 (0.7)	0.2 (0.6)	0.046
Visual perception (VPER)	−0.1 (0.7)	0.3 (0.6)	0.013
Visual construction (VCON)	−0.1 (0.9)	0.4 (0.6)	0.009

Note: Results are displayed as 'mean (standard deviation)' except for sex and Hoehn & Yahr score, which are shown respectively as 'number of males (% of males)' and as 'median (range)'. High- and Low-contrast VA are measured as the number of letters correctly identified by participant (denoted as "no. of letters"). Visual outcomes were converted to *z*-scores and averaged to obtain composite scores of each visual domain.
Abbreviations: iPD, idiopathic Parkinson's disease; LEDD, levodopa equivalent daily dose; MoCA, Montreal Cognitive Assessment; UPDRS, Unified Parkinson's Disease Rating Scale; VA, Visual Acuity.

although the percentage of males was significantly lower in the latter group. In the patients, the median disease duration was 6.1 years, their median Hoehn & Yahr score was 2.0, and the median UPDRS III score was 26.9. In the majority, the disease onset occurred between 55 and 65 years of age, although 10 patients (23.8%) were early onset iPD (disease onset between 21 and 50 years of age) with negative genetic testing (see Section 2). As expected, iPD patients showed a significantly lower cognitive score (MoCA) and worse visual outcomes than controls, especially in LCVA and visual construction tests. A total of seven patients (16.7%) had a history of visual hallucinations.

3.2 | Amygdala Atrophy as a Central Role for Visual Disability in iPD

The common intersection of the four association maps for visual outcomes and gray matter volume, the *visualROI*, is represented in Figure 1. A full anatomical characterization of the *visualROI* is given in Table 2. Remarkably, *visualROI* was preferably located in ventral regions of the brain, rather than primary visual-processing areas. Approximately, 50% of the *visualROI* volume was found in the amygdala bilaterally (32% left and 15% right) and 20% in the left olfactory cortex, hippocampus, and superior temporal gyrus. In fact, the *visualROI* occupied a large part of the volume of the amygdala, especially on the left hemisphere (63% in the left and 25% in the right amygdala).

Interestingly, when we computed the associations between disease duration and brain volume, we found that disease duration was associated with several, mainly temporal-sided regions, including the left temporal superior, middle, and supramarginal lobes but not with the amygdala volume—the main structure within the *visualROI*.

The voxel-level association maps for the four visual domains (LCVA, VPERC, VAPS, and VCONS) demonstrated significant correspondence with traditional visual regions, including the thalamus, calcarine, fusiform, lingual, and inferior, middle, and superior occipital cortices (see detailed results in Tables S1–S4). For example, VCONS displayed a notable overlap with the lingual (29.94%), occipital inferior (34.35%), and fusiform (23.96%) regions, while VAPS was strongly associated with the calcarine (27.22%) and lingual (14.84%) regions. LCVA also showed substantial contributions from the thalamus (31.05%) and lingual (16.29%) regions. These findings confirm that traditional visual regions are represented in the voxel-level association maps of all four visual domains. However, when analyzing the intersection of the four voxel-level association maps, the resulting *visualROI* did not include any of these traditional visual regions. Instead, the *visualROI* primarily comprised subcortical and limbic structures, such as the amygdala, olfactory cortex, and superior temporal gyrus. This highlights the distinct role of these regions in integrating visual functions in PD and underscores the amygdala's central role in early visual dysfunctions.

3.3 | Disruption of Functional Connectivity Between Amygdala and Visual Networks in iPD

We next analyzed the FC of *visualROI* with the main brain networks and their corresponding connectome layout (Figure 2). In controls, *visualROI* presented a strong positive FC with lateral

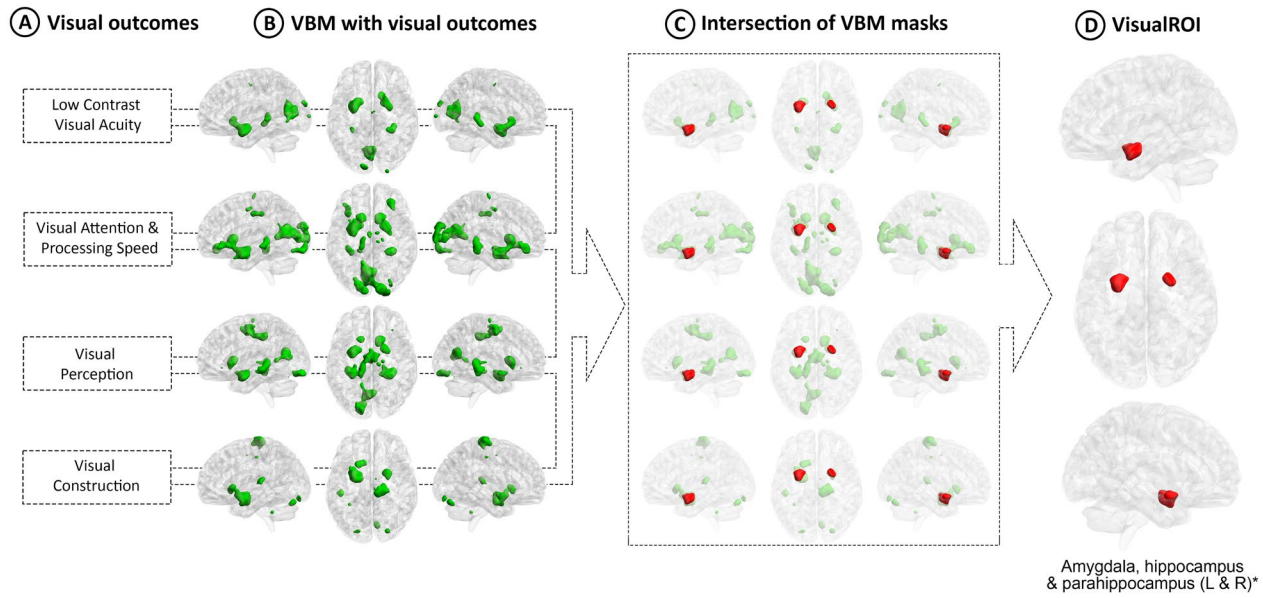

FIGURE 1 | Anatomical characterization of the *visualROI* using voxel-level association maps of gray matter volume and visual outcomes. (A) Visual outcomes. Low-contrast visual acuity was measured as the total number of letters correctly identified on Sloan 2.5% charts. The individual values of visual attention & processing speed and visual perception were obtained using composite scores that included different neuropsychological tests for each of the two domains (see Section 2). The visual construction value was obtained from the Clock Drawing Test score calculated with the Cacho y García scoring method. All four visual outcomes were computed as z-scores. (B) Voxel-level association maps for gray matter volume and each of the four visual outcomes, computed by means of linear regression controlling for age and head size. (C) Intersection of the four association maps, and (D) The determination of the *visualROI*, resulting from the intersection of the maps in C, and consisting of 4 clusters of mainly subcortical gray matter, 2 per cerebral hemisphere, which included the amygdala, hippocampus and parahippocampus on both sides. See Table 2 for a detailed anatomical description of *visualROI*.

TABLE 2 | *VisualROI* in iPD patients.

AAL label	Voxels (*n*)	Volume (mm^3)	MNI X (mm)	MNI Y (mm)	MNI Z (mm)	AAL label percentage (%)	*VisualROI* percentage (%)
Amygdala_L	137	1096	−25	−2	−17	62.27	32.31
Amygdala_R	62	496	25	1	−15	25.00	14.62
Olfactory_L	29	232	−21	6	−16	10.36	6.84
Hippocampus_L	23	184	−28	−7	−18	2.47	5.42
Templ_Pole_Sup_L	21	168	−28	5	−22	1.63	4.95

Note: Only the clusters with a size greater than 10 voxels and that are statistically significant (p-FDR < 0.05) are shown. The *visualROI* is described anatomically in iPD patients using the labels from the AAL brain MRI atlas. *VisualROI* is defined as the significant clusters of gray matter volume loss associated with visual outcomes in iPD patients. The clusters that form the *visualROI* correspond to the intersection of four statistic maps, each corresponding to the association map between voxel-level volumetric patterns and each of the four visual outcomes (low contrast acuity, visual attention & processing speed, visual perception, and visual construction). The table shows the size of the *visualROI* within each AAL label in number of voxels (*n*) and volume (mm^3), the peak MNI coordinates of the *visualROI* within each AAL label, the percentage of each AAL label that is part of the *visualROI* ("AAL label percentage"), the percentage of the *visualROI* within each AAL label ("*VisualROI* percentage").
Abbreviations: AAL, automated anatomical labeling; L, left; MNI, Montreal Neurological Institute; R, right.

sensorimotor networks bilaterally and a moderate positive FC with medial and lateral (left and right) visual networks, language networks (left and rightposterior superior temporal gyri and right inferior frontal gyrus), salience networks (left and right supramarginal gyri, anterior insula, and anterior cingulate cortex), and dorsal attention network (left frontal eye field) (Figure 2A). In the *visualROI* connectome layout of iPD, there were important differences compared to controls (Figure 2B). First, we observed a disruption of the FC of the *visualROI* with both medial and lateral visual networks bilaterally, with the dorsal attention network (frontal eye field left), with the language network (left and right posterior superior temporal gyri), and with a part of the salience network (left and right supramarginal gyri). Second, in iPD, significant connections of the *visual*ROI emerged with the default mode network (medial prefrontal cortex) and salience network (anterior cingulate cortex and anterior insula left and right). More importantly, we determined that the reduced connectivity between *visualROI* and visual networks (medial and both lateral) in iPD was the only significant connectivity difference (Figure 2C) compared to controls after correcting for multiple comparisons.

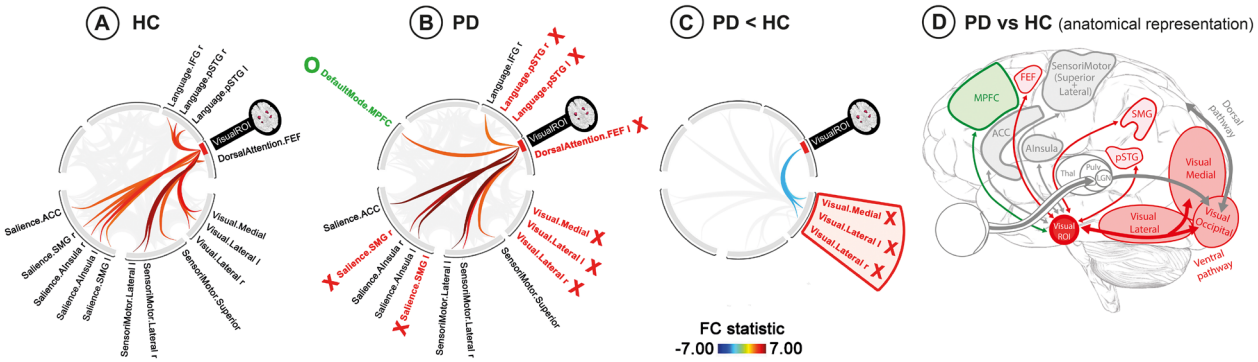

FIGURE 2 | Differences in resting-state functional connectivity (FC) connectome layout of *visualROI* between PD and controls. The figure illustrates the resting-state FC patterns of the *visualROI* across different groups and contrasts. Panel A shows the FC connectome for healthy controls (HC), while panel B displays the FC connectome for idiopathic Parkinson's disease (iPD) patients. Panel C (PD<HC) highlights the statitiscally significant differences in connectivity between iPD and HC. Panel D (PD vs. HC) provides a schematic anatomical representation of the regions of interest (ROIs) and the networks affected in PD, depicted as a diagram. The names surrounding the three rings correspond to pairs of functional brain networks with significant connectivity ($p < 0.05$) for each group or contrast (HC, iPD, or iPD vs. HC), after correction for multiple comparisons (see Section 2). The color scale of the links indicates the value of the FC statistic, reflecting both direction (positive or negative) and magnitude (see Section 2 for details). In panel B, ROIs with statistically significant connections to the visual ROI in both iPD and controls are shown in black text. The green text highlights the ROI (DefaultMode.MPFC) with significant connectivity to the visualROI exclusively in iPD, while red text indicates ROIs with connectivity to the *visualROI* that become non-significant in iPD (significant in controls). In panel D, ROIs with significantly reduced connectivity to the *visualROI* in iPD compared to controls are shown in red. For a detailed description of these results, refer to the Results section. ACC, Anterior Cingulate Cortex; SMG, Supra Marginal Gyrus; AInsula, Anterior Insula; FEF, Frontal Eye Field; pSTG, Posterior Superior Temporal Gyrus; IFG, Inferior Frontal Gyrus; MPFC, Medial Prefrontal Cortex; Thal, Thalamus; Pulv, Pulvinar; LGN, Lateral Geniculate Nucleus.

3.4 | Retinal and Amygdala Atrophy in iPD: Evidence for a Two-Phase Neurodegeneration Model Aligned with Braak's Stages

After family wise error (FEW)-correction, a statistically significant positive association was found in iPD and not in controls between the parafoveal GCIPL thickness and the volume of several gray matter regions of the frontal and ventral brain, mainly subcortical structures (*retinalROI*) (Figure 3). More specifically, *retinalROI* mainly coincided with bilateral basal ganglia and thalamus (17.9% and 17.5% of *retinalROI* volume, respectively) to a lesser extent with frontal cortical regions (12.8%), hippocampus and parahippocampus (9.4%), and cingulum (6.1%) and with the primary visual cortex (calcarine sulcus) (4.1%) and visual associative cortex (fusiform and lingual gyri) (4.0%) (Figure 3 and Table S5). More specifically, among the structures of the basal ganglia within the *retinalROI*, the caudate nuclei stood out (10.6%), followed by the amygdala (5.2%) and the putamen (2.0%). Of note, approximately, 50% of the amygdala volume was included in the resulting *retinalROI* (56.8% of left and 45.6% of right amygdala). To investigate to what extent *visualROI* was anatomically related to *retinalROI*, we computed the intersection between both ROIs and confirmed that there was a partial but clear overlap, especially with the left and right amygdalae, since 54% of *retinalROI–visualROI* intersection corresponded to amygdala (Table S5). Finally, analysis of covariance of the *retinalROI* regions revealed three primary clusters: (1) thalamic nuclei, (2) amygdala and visual regions (visual lateral and occipital), and (3) frontal regions (mesocortex (ACC) and frontal attention networks (dlPFC)) (Figure 4A). According to this analysis, retinal thinning was most strongly associated with gray matter volume loss in the frontal cluster. In contrast, amygdala atrophy was most closely associated with volume loss in lateral visual and occipital visual regions. These findings support the hypothesis of a two-phase progression model aligned with Braak's stages (Figure 4B). In the early phase (Braak 1–3), amygdala degeneration leads to disconnection from the ventral visual pathway and extra-geniculate visual pathway, impairing conscious and non-conscious visual processing. In the later phase (Braak 4–5), degeneration extends to the frontal regions and the retina, collectively exacerbating visual dysfunctions and highlighting the amygdala's central role in integrating retinal and cortical pathways. This observation does not imply propagation of pathology from the retina to frontal regions but rather suggests that the timing of significant retinal atrophy aligns with the neurodegeneration of frontal regions occurring in Braak stages 4–5.

4 | Discussion

This study comprehensively evaluates the neuroanatomical basis of visual dysfunction in PD by integrating structural MRI, resting-state functional MRI, and retinal OCT with a detailed assessment of visual function. Although visual outcomes in PD were associated with atrophy in various cortical and subcortical regions, including classic primary and associative visual areas such as the calcarine cortex and medial temporal cortex, our findings highlight amygdala atrophy (*visualROI*) as the common denominator across all visual domains explored. FC analyses further revealed statistically significant disruptions between the amygdala and visual networks in PD compared to controls, underscoring the amygdala's central role in the genesis of visual disability. Moreover, the observed relationships between retinal atrophy, amygdala degeneration, and other brain regions support a two-phase progression model of visual impairments in PD, aligned with Braak's stages. In this amygdala-centric model,

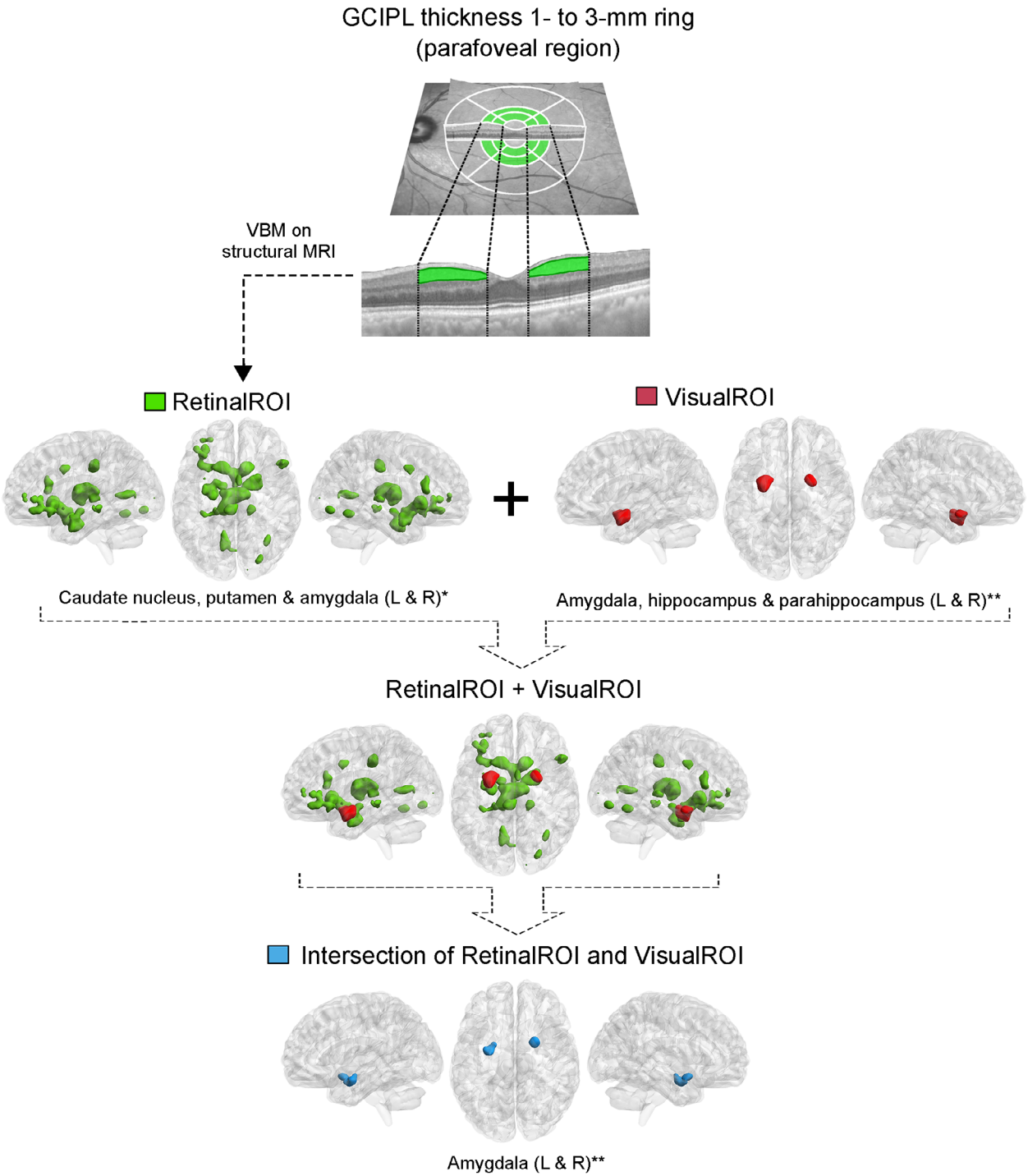

FIGURE 3 | Identification of *retinalROI* and its anatomical relation with *visualROI*. The segmented GCIPL complex in the parafoveal region (1- to 3-mm ring) of the macula is shown at the top in green on a foveal-centered OCT axial slice. The voxel-level association map for gray matter volume and GCIPL thickness in the parafoveal region (1- to 3-mm ring) of the macula (*retinalROI*) is shown at the top leftin green. *RetinalROI* anatomically corresponded mainly to the left and right caudate nucleus, putamen and amygdala. In the upper right part, in red, the *visualROI* map is shown (explained in Section 3 and in Figure 1). The intersection between both maps, *retinalROI* and *visualROI*, shown below in blue, corresponded anatomically with the left and right amygdala (see Section 3 and Table S5 for a more detailed description). GCIPL, Ganglion cell-inner plexiform layer complex.

early amygdala degeneration disrupts visual pathways, including the ventral visual and extrageniculate networks, impairing both conscious and unconscious visual processing (Braak 1–3). In more advanced stages (Braak 4–5), disconnection between the amygdala and frontal regions, combined with retinal neurodegeneration, exacerbates visual disability. This integrative model highlights the amygdala's critical role in the progression of PD-related visual dysfunction and establishes a framework for understanding its structural and functional underpinnings.

While many previous imaging studies focused on visual hallucinations or cognitive impairment, few have examined structural

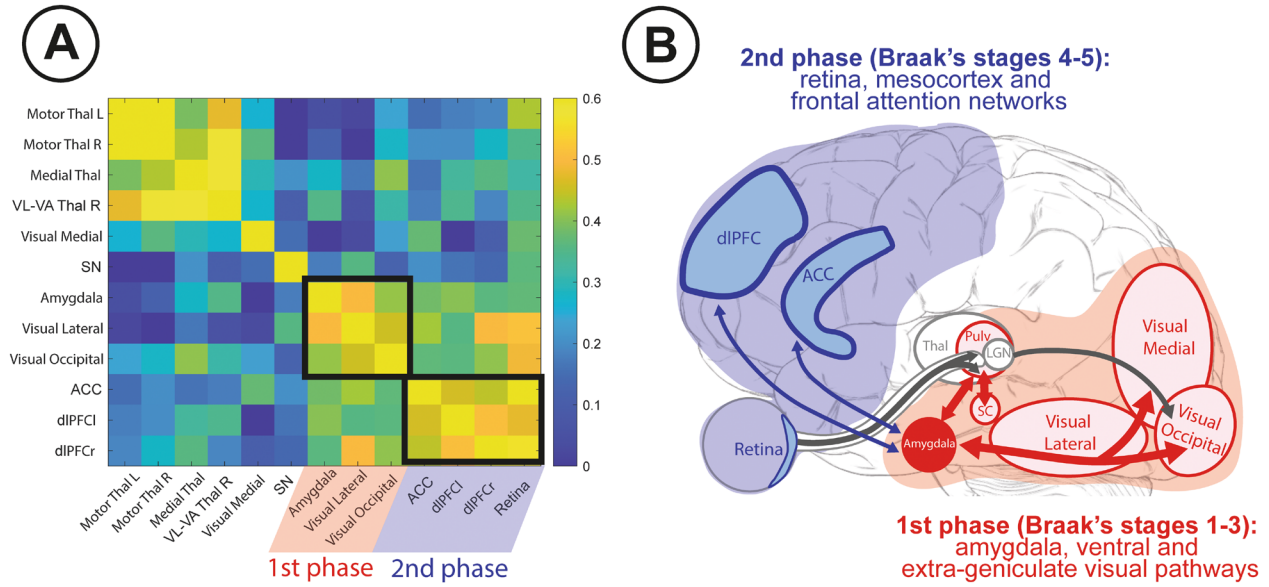

FIGURE 4 | Analysis of covariance of *retinalROI* regions and proposed amygdala-centric two-phase model of visual deficits in Parkinson's disease. In panel A, the correlogram illustrates the analysis of covariance of the *retinalROI* regions, revealing three primary clusters: (1) the thalamic nucleus, (2) the amygdala and visual regions (lateral visual and occipital areas), and (3) frontal regions, including the mesocortex (anterior cingulate cortex, ACC) and frontal attention networks (dorsolateral prefrontal cortex, dlPFC). Retinal thinning was most strongly associated with gray matter volume loss in the frontal cluster, while amygdala atrophy was most closely linked to volume loss in the lateral and occipital visual regions. In panel B, the diagram presents the proposed amygdala-centric model, highlighting amygdala neurodegeneration as a key factor in explaining visual deficits in PD. This model suggests a two-phase progression aligned with Braak's stages: Early phase (Braak 1–3): Amygdala degeneration disrupts connections to the ventral visual pathway and extra-geniculate visual pathway, impairing both conscious and non-conscious visual processing. Later phase (Braak 4–5): Neurodegeneration extends to frontal regions and the retina, exacerbating visual dysfunction. Retinal atrophy aligns with frontal region degeneration during Braak stages 4–5, underscoring the amygdala's central role in integrating retinal and cortical pathways. These findings provide further insight into the mechanisms underlying visual dysfunction in Parkinson's disease, emphasizing the interplay between retinal damage, amygdala degeneration, and disruptions in the lateral, medial visual, and frontal networks. ACC, anterior cingulate cortex; dlPFC, dorso lateral prefrontal cortex; LGN, lateral geniculate nucleus; Medial Thal, medial thalamus; Motor Thal, motor thalamus; Pulv, Pulvinar; SC, superior colliculus; SN, substantia nigra; Thal, thalamus; VL-VA Thal, ventrolateral ventroanterial thalamus.

and functional alterations underlying visual dysfunction in PD. Prior studies reported associations between visuoperceptual and visuospatial deficits in PD and thinning in different cortical regions, including the superior parietal cortex and precuneus [40], lateral parietal and temporal cortices, [42] and left superior temporal parahippocampal and lingual cortices [43]. Building on previous studies, our voxel-level association maps revealed significant correlations in PD between visual outcomes (LCVA, VCONS, VAPS, and VPERC) and atrophy in various primary and associative visual regions, including the lingual gyrus, fusiform gyrus, inferior occipital cortex, calcarine cortex, and thalamus (see Figure 1 and Tables S1–S4). A key distinction of our study, however, is the identification of the amygdala as a shared region of interest (*visualROI*) across multiple visual domains. This integrative finding underscores the amygdala's central role in PD-related visual impairments, providing a unifying neuroanatomical basis for deficits spanning diverse visual functions.

Combined structural and diffusion tensor imaging studies have demonstrated microstructural changes in optic radiations connecting the lateral geniculate nucleus and V2 as well as reduced visual cortical volume and chiasmatic area [44]. However, due to the absence of diffusion imaging in our study, we could not evaluate the relationship between visual tract microstructural damage and visual outcomes. Resting-state fMRI studies in PD consistently show reduced FC between visual networks and other major brain networks [55, 56]. Task-based fMRI has provided further insights into visual dysfunction mechanisms. For example, impairments in optic flow processing, linked to gait disturbances, are associated with reduced activation in the MT+ region and altered activity in the cingulate sulcus [45]. Abnormal wide-field optic flow processing in PD has also been linked to reduced visual cortex activation and increased connectivity between V5, the pre-supplementary motor area, and the cerebellum [47]. Additionally, visuospatial attention tasks reveal diminished cortical connectivity modulation in regions such as the superior frontal gyrus, opercular cortex, and parieto-occipital cortex [57], suggesting that impaired interactions between attentional and visual networks contribute to visual dysfunction in PD. Disruptions in contrast luminance perception have also been associated with abnormal superior colliculus responses [46], implicating the extrageniculate visual pathway and its connections to the amygdala.

While these imaging findings have advanced our understanding of the neural mechanisms underlying visual dysfunction in PD, inconsistencies across studies reveal significant methodological challenges. Variations in imaging analysis techniques, cognitive tests, and task designs have led to divergent results. In some cases, tests evaluating visuospatial and visuoperceptual

functions were categorized under other cognitive domains, potentially obscuring associations with visual processing. Unlike prior studies that primarily focused on the anatomical and functional correlates of single visual functions or tasks, our study adopted a more integrative approach. This approach allowed us to identify a more comprehensive and generalizable neuroanatomical substrate for visual disability in PD, offering insights that go beyond isolated visual functions. By integrating voxel-level association maps across four visual domains, we identified the amygdala (*visualROI*) as a shared hub consistently linked to visual impairments. This finding, coupled with disrupted ventral visual network connectivity, highlights the amygdala's central role in PD-related visual dysfunction, providing a more comprehensive and generalizable neuroanatomical framework. The amygdala serves as a hub for visual-emotional integration, modulating attention, prioritizing emotionally relevant stimuli, and contributing to associative learning [58–60]. It connects extensively with both the cortical "high road" (LGN-striate cortex-occipitotemporal cortex-amygdala) and the subcortical "low road" (superior colliculus-pulvinar-amygdala), enabling both conscious and subconscious processing of visual stimuli [61, 62]. This duality reflects the amygdala's evolutionary role in mediating emotional and fear responses. Neurons in the basolateral amygdala (BLA) play a key role in visual learning and attention [61], while the centromedial nucleus focuses awareness on emotionally salient stimuli [63]. Evidence from blindsight patients and studies of non-mammalian vertebrates further supports the critical role of the superior colliculus and pulvinar in automatic, non-conscious emotional visual processing [64, 65].

Unlike PD, visual deficits in healthy older adults are primarily linked to age-related declines in the retina or the visual pathway (up to the occipital cortex), with relatively modest amygdala involvement [66]. Previous studies of aging cohorts have reported limited volumetric reductions in the amygdala [67] and post-mortem measurements based on histological staining reveal no significant effect of age on amygdala volume [68]. From a functional point of view, fMRI studies in healthy population support that the amygdala functions similarly in healthy older adults as it does in younger adults [69].

In PD, the amygdala is an early target of Lewy pathology, with neurodegeneration occurring from prodromal stages [70]. Reduced amygdala volume has been observed even in de novo PD patients [71], and the density of Lewy bodies in the amygdala has been found to correlate with the presence of visual alterations in non-demented PD patients [72]. In line with our findings, other studies also found that the degree of neurodegeneration of the amygdala (neuron loss or atrophy) was not associated with the duration of the disease [72, 73]. All of this supports the idea that amygdala neurodegeneration in PD is an early phenomenon that does not further progress later on. The BLA is particularly vulnerable in PD, showing hypoconnectivity with temporal and frontal regions, including the fusiform gyrus and ventromedial prefrontal cortex [74]. These disruptions are linked to cognitive, emotional, and olfactory deficits, underscoring the BLA's role in ventral visual network integration. The BLA serves as a critical hub for multimodal sensory integration, receiving inputs from temporal lobe structures and neuromodulatory systems, including noradrenergic, dopaminergic, and cholinergic pathways originating from the locus coeruleus, ventral tegmental area, and basal forebrain, respectively [75, 76]. Noradrenergic activation of the BLA, triggered by emotionally arousing stimuli, plays a key role in strengthening long-term memory and facilitating object recognition memory, which primarily relies on cortical structures. Notably, the locus coeruleus is among the earliest structures affected in PD, and its degeneration may contribute to early BLA dysfunction, providing a mechanistic explanation for the amygdala's involvement in visual deficits observed in PD.

Our findings align with the "blind to blindsight" hypothesis, which posits that PD patients experience impaired unconscious visual processing and emotional recognition despite preserved conscious vision [77]. This contrasts with classical blindsight, where unconscious visual perception remains intact despite cortical damage [64]. This hypothesis highlights dysfunction in two parallel circuits: (1) the retino-colliculo-thalamo-amygdala pathway, mediating non-conscious emotional processing, and (2) the retino-geniculo-extrastriate pathway, supporting conscious visual identification and spatial awareness. Early amygdala degeneration in PD disrupts both pathways, leading to deficits in motion detection, emotional face recognition, and visual localization.

Thus, our findings reinforce the concept of a 'silent amygdala' in PD, where Lewy pathology leads to degeneration and hypoconnectivity, disrupting both conscious and non-conscious visual processing pathways.

The selective vulnerability of the amygdala in PD differentiates it from normal aging patterns, underscoring its critical role in early disease-related changes [72]. The results align with Braak's staging, suggesting that the amygdala is affected in early PD, consistent with the brain-first subtype. As a target of Lewy pathology, early amygdala degeneration disrupts both structural and functional connections with ventral visual stream (supporting conscious object recognition and discrimination), extrageniculate pathway (mediating non-conscious emotional responses and reflexive visual behaviors), higher-order visual networks (including occipital, medial, and lateral areas, which handle complex visual processing) and attention networks (such as the anterior cingulate cortex and precuneus, critical for higher-order tasks like visual attention).

This study has some limitations. Most patients were on dopaminergic and non-dopaminergic medications, which may influence visual outcomes. While dopaminergic effects were controlled by assessing patients in the ON state, non-dopaminergic influences were not fully accounted for. Additionally, while we observed associations between retinal thinning and amygdala atrophy, the underlying mechanisms remain unclear, warranting further investigation. Finally, visual and neuropsychological tests used in this study extend beyond isolated visual assessments, involving multiple cognitive domains, including language processing. Reduced connectivity between the amygdala and the posterior superior temporal gyrus—a key language region—further underscores the impact of multimodal integration deficits in PD. These findings suggest that visual tasks often engage broader cognitive and sensory networks, which are disrupted by PD-related neurodegeneration.

Overall, this study supports a novel amygdala-centric two-phase model of visual dysfunction in PD, aligned with Braak's stages. In the early phase (Braak 1–3), amygdala degeneration disrupts its connections with ventral visual and extrageniculate pathways, impairing conscious and unconscious visual processing. In the later phase (Braak 4–5), degeneration extends to the retina and frontal regions, exacerbating visual deficits. Reduced FC between the amygdala and anterior cingulate cortex, superior temporal gyrus, and other frontal areas further highlights the impact of amygdala-frontal disconnection in advanced stages. Our model also emphasizes a parallel retinal-brain neurodegeneration axis, wherein shared susceptibility between retinal and subcortical structures contributes to visual impairment. The observed correlation between parafoveal GCIPL thinning and amygdala atrophy supports this hypothesis. The early degeneration of the amygdala likely reflects its vulnerability to Lewy pathology, consistent with the brain-first subtype of PD.

Author Contributions

Asier Erramuzpe: data analysis, drafting, editing final version of manuscript. Ane Murueta-Goyena: data analysis, drafting, editing final version of manuscript. Antonio Jimenez-Marin: data analysis; Marian Acera: data acquisition. Sara Teijeira-Portas: data acquisition. Rocío Del Pino: data acquisition. Tamara Fernández-Valle: data acquisition. Ibai Diez: data analysis. Unai Sainz: data analysis. Naroa Ibarretxe-Bilbao: editing of final version of manuscript. Unai Ayala: data analysis, editing final version of manuscript. Maitane Barrenechea: data analysis, editing final version of manuscript. Alberto Cabrera-Zubizarreta: data acquisition. Jesús Cortés: data analysis, editing final version of manuscript. Juan Carlos Gómez-Esteban: editing final version of manuscript. Iñigo Gabilondo: conception/design, drafting, editing final version of manuscript.

Acknowledgments

The authors want to thank all the patients and participants involved in the study.

Conflicts of Interest

This study was cofunded by the Michael J. Fox Foundation (RRIA [Rapid Response Innovation Awards] 2014 Program, grant ID: 10189), the Carlos III Health Institute, and the European Union (ERDF/ESF, "A Way to Make Europe"/"Investing in Your Future") through the projects PI14/00679 and PI16/00005; and the Department of Health of the Basque Government through the projects 2016111009 and 2020333033. Iñigo Gabilondo contract was funded by an Ikerbasque Fellow contract from Ikerbasque, the Basque Foundation for Science, and by a Juan Rodes grant JR15/00008 from the Carlos III Health Institute. Asier Erramuzpe contract was funded by The Spanish Ministry of Science and Innovation, grant "RYC2021-032390-I" "RYC2022-035429-I" and Ikerbasque, the Basque Foundation for Science. Antonio Jimenez-Marin contract was funded by a predoctoral grant from the Basque Government "PRE_2019_1_0070". Jesús Cortés was funded by Ikerbasque, the Basque Foundation for Science. For the rest of authors, none have received any funding from any institution, including personal relationships, interests, grants, employment, affiliations, patents, inventions, honoraria, consultancies, royalties, stock options/ownership, or expert testimony for the last 12 months. The authors report no competing interests.

Data Availability Statement

The data and the source-code of the analysis that support the findings of this study will be available after publication from the corresponding author, upon reasonable request.

References

1. W. H. Whitfield, G. Q. Barr, M. J. Khayata, et al., "Contrast Sensitivity Visual Acuity in REM Sleep Behavior Disorder: A Comparison with and Without Parkinson Disease," *Journal of Clinical Sleep Medicine* 16, no. 3 (2020): 385–388.

2. Y. Li, H. Zhang, W. Mao, et al., "Visual Dysfunction in Patients with Idiopathic Rapid Eye Movement Sleep Behavior Disorder," *Neuroscience Letters* 709 (2019): 134360.

3. L. A. Leyland, F. D. Bremner, R. Mahmood, et al., "Visual Tests Predict Dementia Risk in Parkinson Disease," *Neurology Clinical Practice* 10, no. 1 (2020): 29–39.

4. A. Murueta-Goyena, R. Del Pino, M. Galdós, et al., "Retinal Thickness Predicts the Risk of Cognitive Decline in Parkinson Disease," *Annals of Neurology* 89 (2020): 165–176.

5. I. Bodis-Wollner and M. D. Yahr, "Measurements of Visual Evoked Potentials in Parkinson's Disease," *Brain* 101, no. 4 (1978): 661–671.

6. A. Cronin-Golomb and A. E. Braun, "Visuospatial Dysfunction and Problem Solving in Parkinson's Disease," *Neuropsychology* 11, no. 1 (1997): 44–52.

7. M. M. Amick, A. Cronin-Golomb, and G. C. Gilmore, "Visual Processing of Rapidly Presented Stimuli is Normalized in Parkinson's Disease When Proximal Stimulus Strength is Enhanced," *Vision Research* 43, no. 26 (2003): 2827–2835.

8. S. Davidsdottir, A. Cronin-Golomb, and A. Lee, "Visual and Spatial Symptoms in Parkinson's Disease," *Vision Research* 45, no. 10 (2005): 1285–1296.

9. M. M. Amick, H. E. Schendan, G. Ganis, and A. Cronin-Golomb, "Frontostriatal Circuits are Necessary for Visuomotor Transformation: Mental Rotation in Parkinson's Disease," *Neuropsychologia* 44, no. 3 (2006): 339–349.

10. U. S. Clark, S. Neargarder, and A. Cronin-Golomb, "Specific Impairments in the Recognition of Emotional Facial Expressions in Parkinson's Disease," *Neuropsychologia* 46, no. 9 (2008): 2300–2309.

11. J. P. Harris, J. E. Calvert, and O. T. Phillipson, "Processing of Spatial Contrast in Peripheral Vision in Parkinson's Disease," *Brain* 115, no. Pt 5 (1992): 1447–1457.

12. S. A. McDowell and J. P. Harris, "Visual Problems in Parkinson's Disease: A Questionnaire Survey," *Behavioural Neurology* 10, no. 2 (1997): 77–81.

13. A. C. Lee, J. P. Harris, and J. E. Calvert, "Impairments of Mental Rotation in Parkinson's Disease," *Neuropsychologia* 36, no. 1 (1998): 109–114.

14. J. G. Smith, J. P. Harris, S. Khan, E. A. Atkinson, M. S. Fowler, and R. P. Gregory, "Perceptual Bias for Affective and Nonaffective Information in Asymmetric Parkinson's Disease," *Neuropsychology* 24, no. 4 (2010): 443–456.

15. M. M. Amick, I. N. Miller, S. Neargarder, and A. Cronin-Golomb, "Web-Based Assessment of Visual and Visuospatial Symptoms in Parkinson's Disease," *Parkinsons Disease* 2012 (2012): 564812.

16. S. Davidsdottir, R. Wagenaar, D. Young, and A. Cronin-Golomb, "Impact of Optic Flow Perception and Egocentric Coordinates on Veering in Parkinson's Disease," *Brain* 131, no. Pt 11 (2008): 2882–2893.

17. D. E. Young, R. C. Wagenaar, C. C. Lin, et al., "Visuospatial Perception and Navigation in Parkinson's Disease," *Vision Research* 50, no. 23 (2010): 2495–2504.

18. C. C. Lin, R. C. Wagenaar, D. Young, et al., "Effects of Parkinson's Disease on Optic Flow Perception for Heading Direction During Navigation," *Experimental Brain Research* 232, no. 4 (2014): 1343–1355.

19. C. C. Lin and R. C. Wagenaar, "The Impact of Walking Speed on Interlimb Coordination in Individuals with Parkinson's disease," *Journal of Physical Therapy Science* 30, no. 5 (2018): 658–662.

20. D. J. Norton, A. Jaywant, X. Gallart-Palau, and A. Cronin-Golomb, "Normal Discrimination of Spatial Frequency and Contrast Across Visual Hemifields in Left-Onset Parkinson's Disease: Evidence Against Perceptual Hemifield Biases," *Vision Research* 107 (2015): 94–100.

21. A. Jaywant, T. D. Ellis, S. Roy, C. C. Lin, S. Neargarder, and A. Cronin-Golomb, "Randomized Controlled Trial of a Home-Based Action Observation Intervention to Improve Walking in Parkinson Disease," *Archives of Physical Medicine and Rehabilitation* 97, no. 5 (2016): 665–673.

22. A. Jaywant, V. Wasserman, M. Kemppainen, S. Neargarder, and A. Cronin-Golomb, "Perception of Communicative and Non-Communicative Motion-Defined Gestures in Parkinson's Disease," *Journal of the International Neuropsychological Society* 22, no. 5 (2016): 540–550.

23. A. Jaywant, M. Shiffrar, S. Roy, and A. Cronin-Golomb, "Impaired Perception of Biological Motion in Parkinson's Disease," *Neuropsychology* 30, no. 6 (2016): 720–730.

24. R. D. Salazar, K. L. M. Moon, S. Neargarder, and A. Cronin-Golomb, "Spatial Judgment in Parkinson's Disease: Contributions of Attentional and Executive Dysfunction," *Behavioral Neuroscience* 133, no. 4 (2019): 350–360.

25. C. C. Wu, B. Cao, V. Dali, et al., "Eye Movement Control During Visual Pursuit in Parkinson's Disease," *PeerJ* 6 (2018): e5442.

26. J. Y. Lee, A. Martin-Bastida, A. Murueta-Goyena, et al., "Multimodal Brain and Retinal Imaging of Dopaminergic Degeneration in Parkinson Disease," *Nature Reviews. Neurology* 18, no. 4 (2022): 203–220.

27. V. Polo, M. Satue, M. J. Rodrigo, et al., "Visual Dysfunction and its Correlation with Retinal Changes in Patients with Parkinson's Disease: An Observational Cross-Sectional Study," *BMJ Open* 6, no. 5 (2016): e009658.

28. A. Murueta-Goyena, R. Del Pino, P. Reyero, et al., "Parafoveal Thinning of Inner Retina is Associated with Visual Dysfunction in Lewy Body Diseases," *Movement Disorders* 34, no. 9 (2019): 1315–1324.

29. I. Bodis-Wollner, "Visual Electrophysiology in Parkinson's Disease: PERG, VEP and visual P300," *Clinical Electroencephalography* 28, no. 3 (1997): 143–147.

30. L. Huang, D. Zhang, J. Ji, Y. Wang, and R. Zhang, "Central Retina Changes in Parkinson's Disease: A Systematic Review and Meta-Analysis," *Journal of Neurology* 268, no. 12 (2020): 4646–4654.

31. L. Veys, M. Vandenabeele, I. Ortuno-Lizaran, et al., "Retinal Alpha-Synuclein Deposits in Parkinson's Disease Patients and Animal Models," *Acta Neuropathologica* 137, no. 3 (2019): 379–395.

32. I. Ortuño-Lizarán, X. Sánchez-Sáez, P. Lax, et al., "Dopaminergic Retinal Cell Loss and Visual Dysfunction in Parkinson Disease," *Annals of Neurology* 88, no. 5 (2020): 893–906.

33. J. T. Hutton, J. L. Morris, and J. W. Elias, "Levodopa Improves Spatial Contrast Sensitivity in Parkinson's Disease," *Archives of Neurology* 50, no. 7 (1993): 721–724.

34. D. Weintraub, J. Doshi, D. Koka, et al., "Neurodegeneration Across Stages of Cognitive Decline in Parkinson Disease," *Archives of Neurology* 68, no. 12 (2011): 1562–1568.

35. E. J. Burton, I. G. McKeith, D. J. Burn, E. D. Williams, and J. T. O'Brien, "Cerebral Atrophy in Parkinson's Disease with and Without Dementia: A Comparison with Alzheimer's Disease, Dementia with Lewy Bodies and Controls," *Brain* 127, no. Pt 4 (2004): 791–800.

36. D. Garcia-Garcia, P. Clavero, C. Gasca Salas, et al., "Posterior Parietooccipital Hypometabolism May Differentiate Mild Cognitive Impairment from Dementia in Parkinson's Disease," *European Journal of Nuclear Medicine and Molecular Imaging* 39, no. 11 (2012): 1767–1777.

37. P. Borghammer, "Perfusion and Metabolism Imaging Studies in Parkinson's Disease," *Danish Medical Journal* 59, no. 6 (2012): B4466.

38. K. Nie, Y. Zhang, B. Huang, et al., "Marked N-Acetylaspartate and Choline Metabolite Changes in Parkinson's Disease Patients with Mild Cognitive Impairment," *Parkinsonism & Related Disorders* 19, no. 3 (2013): 329–334.

39. H. Braak, K. Del Tredici, U. Rub, R. A. de Vos, E. N. Jansen Steur, and E. Braak, "Staging of Brain Pathology Related to Sporadic Parkinson's disease," *Neurobiology of Aging* 24, no. 2 (2003): 197–211.

40. J. B. Pereira, P. Svenningsson, D. Weintraub, et al., "Initial Cognitive Decline is Associated with Cortical Thinning in Early Parkinson disease," *Neurology* 82, no. 22 (2014): 2017–2025.

41. E. Mak, J. Zhou, L. C. Tan, W. L. Au, Y. Y. Sitoh, and N. Kandiah, "Cognitive Deficits in Mild Parkinson's Disease are Associated with Distinct Areas of Grey Matter Atrophy," *Journal of Neurology, Neurosurgery, and Psychiatry* 85, no. 5 (2014): 576–580.

42. A. I. Garcia-Diaz, B. Segura, H. C. Baggio, et al., "Structural Brain Correlations of Visuospatial and Visuoperceptual Tests in Parkinson's Disease," *Journal of the International Neuropsychological Society* 24, no. 1 (2018): 33–44.

43. A. I. Garcia-Diaz, B. Segura, H. C. Baggio, et al., "Cortical Thinning Correlates of Changes in Visuospatial and Visuoperceptual Performance in Parkinson's Disease: A 4-Year Follow-Up," *Parkinsonism & Related Disorders* 46 (2018): 62–68.

44. A. Arrigo, A. Calamuneri, D. Milardi, et al., "Visual System Involvement in Patients with Newly Diagnosed Parkinson Disease," *Radiology* 285, no. 3 (2017): 885–895.

45. D. Putcha, R. S. Ross, M. L. Rosen, et al., "Functional Correlates of Optic Flow Motion Processing in Parkinson's Disease," *Frontiers in Integrative Neuroscience* 8 (2014): 57.

46. E. Bellot, L. Kauffmann, V. Coizet, S. Meoni, E. Moro, and M. Dojat, "Effective Connectivity in Subcortical Visual Structures in De Novo Patients with Parkinson's Disease," *Neuroimage: Clinical* 33 (2022): 102906.

47. A. van der Hoorn, R. J. Renken, K. L. Leenders, and B. M. de Jong, "Parkinson-Related Changes of Activation in Visuomotor Brain Regions During Perceived Forward Self-Motion," *PLoS One* 9, no. 4 (2014): e95861.

48. A. J. Hughes, S. E. Daniel, L. Kilford, and A. J. Lees, "Accuracy of Clinical Diagnosis of Idiopathic Parkinson's Disease: A Clinico-Pathological Study of 100 cases," *Journal of Neurology, Neurosurgery, and Psychiatry* 55, no. 3 (1992): 181–184.

49. A. Murueta-Goyena, R. Del Pino, M. Galdos, et al., "Retinal Thickness Predicts the Risk of Cognitive Decline in Parkinson Disease," *Annals of Neurology* 89, no. 1 (2021): 165–176.

50. U. P. Mosimann, D. Collerton, R. Dudley, et al., "A Semi-Structured Interview to Assess Visual Hallucinations in Older People," *International Journal of Geriatric Psychiatry* 23, no. 7 (2008): 712–718.

51. P. Tewarie, L. Balk, F. Costello, et al., "The OSCAR-IB Consensus Criteria for Retinal OCT Quality Assessment," *PLoS One* 7, no. 4 (2012): e34823.

52. A. Cruz-Herranz, L. J. Balk, T. Oberwahrenbrock, et al., "The APOSTEL Recommendations for Reporting Quantitative Optical Coherence Tomography Studies," *Neurology* 86, no. 24 (2016): 2303–2309.

53. S. Whitfield-Gabrieli and A. Nieto-Castanon, "Conn: A Functional Connectivity Toolbox for Correlated and Anticorrelated Brain Networks," *Brain Connectivity* 2, no. 3 (2012): 125–141.

54. A. Nieto-Castanon and S. Whitfield-Gabrieli, "CONN Functional Connectivity Toolbox: RRID SCR_009550. Version version. 2022;22".

55. M. Gottlich, T. F. Munte, M. Heldmann, M. Kasten, J. Hagenah, and U. M. Kramer, "Altered Resting State Brain Networks in Parkinson's Disease," *PLoS One* 8, no. 10 (2013): e77336.

56. M. Filippi, E. Sarasso, and F. Agosta, "Resting-State Functional MRI in Parkinsonian Syndromes," *Movement Disorders Clinical Practice* 6, no. 2 (2019): 104–117.

57. D. Vereb, M. A. Kovacs, S. Antal, et al., "Modulation of Cortical Resting State Functional Connectivity During a Visuospatial Attention Task in Parkinson's Disease," *Frontiers in Neurology* 13 (2022): 927481.

58. D. Bzdok, A. R. Laird, K. Zilles, P. T. Fox, and S. B. Eickhoff, "An Investigation of the Structural, Connectional, and Functional Subspecialization in the Human Amygdala," *Human Brain Mapping* 34, no. 12 (2013): 3247–3266.

59. G. Gainotti, "Unconscious Processing of Emotions and the Right Hemisphere," *Handbook of Clinical Neurology* 183 (2021): 27–46.

60. E. E. Benarroch, "The Amygdala: Functional Organization and Involvement in Neurologic Disorders," *Neurology* 84, no. 3 (2015): 313–324, https://doi.org/10.1212/WNL.0000000000001171.

61. D. J. Kravitz, K. S. Saleem, C. I. Baker, L. G. Ungerleider, and M. Mishkin, "The Ventral Visual Pathway: An Expanded Neural Framework for the Processing of Object Quality," *Trends in Cognitive Sciences* 17, no. 1 (2013): 26–49.

62. M. Tamietto, P. Pullens, B. de Gelder, L. Weiskrantz, and R. Goebel, "Subcortical Connections to Human Amygdala and Changes Following Destruction of the Visual Cortex," *Current Biology* 22, no. 15 (2012): 1449–1455.

63. S. Duncan and L. F. Barrett, "The Role of the Amygdala in Visual Awareness," *Trends in Cognitive Sciences* 11, no. 5 (2007): 190–192.

64. S. Ajina and H. Bridge, "Blindsight and Unconscious Vision: What They Teach Us about the Human Visual System," *Neuroscientist* 23, no. 5 (2016): 529–541.

65. L. Pessoa and R. Adolphs, "Emotion Processing and the Amygdala: From a 'low road' to 'many roads' of Evaluating Biological Significance," *Nature Reviews. Neuroscience* 11, no. 11 (2010): 773–783.

66. D. Garzone, R. P. Finger, M. M. Mauschitz, et al., "Visual Impairment and Retinal and Brain Neurodegeneration: A Population-Based Study," *Human Brain Mapping* 44, no. 7 (2023): 2701–2711.

67. J. S. Allen, J. Bruss, C. K. Brown, and H. Damasio, "Normal Neuroanatomical Variation Due to Age: The Major Lobes and a Parcellation of the Temporal Region," *Neurobiology of Aging* 26, no. 9 (2005): 1245–1260, discussion 79–82.

68. J. Brabec, A. Rulseh, B. Hoyt, et al., "Volumetry of the Human Amygdala—An Anatomical Study," *Psychiatry Research* 182, no. 1 (2010): 67–72.

69. K. Nashiro, M. Sakaki, and M. Mather, "Age Differences in Brain Activity During Emotion Processing: Reflections of Age-Related Decline or Increased Emotion Regulation?," *Gerontology* 58, no. 2 (2012): 156–163.

70. P. Borghammer, J. Horsager, K. Andersen, et al., "Neuropathological Evidence of Body-First vs. Brain-First Lewy Body Disease," *Neurobiology of Disease* 161 (2021): 105557.

71. Y. Zeighami, S. M. Fereshtehnejad, M. Dadar, et al., "A Clinical-Anatomical Signature of Parkinson's Disease Identified with Partial Least Squares and Magnetic Resonance Imaging," *NeuroImage* 190 (2019): 69–78.

72. A. J. Harding, E. Stimson, J. M. Henderson, and G. M. Halliday, "Clinical Correlates of Selective Pathology in the Amygdala of Patients with Parkinson's Disease," *Brain* 125, no. Pt 11 (2002): 2431–2445.

73. M. Qu, B. Gao, Y. Jiang, et al., "Atrophy Patterns in Hippocampus and Amygdala Subregions of Depressed Patients with Parkinson's Disease," *Brain Imaging and Behavior* 18, no. 3 (2024): 475–484.

74. J. Wang, L. Sun, L. Chen, et al., "Common and Distinct Roles of Amygdala Subregional Functional Connectivity in Non-Motor Symptoms of Parkinson's Disease," *NPJ Parkinsons Disease* 9, no. 1 (2023): 28.

75. Y. F. Chen, Q. Song, P. Colucci, et al., "Basolateral Amygdala Activation Enhances Object Recognition Memory by Inhibiting Anterior Insular Cortex Activity," *Proceedings of the National Academy of Sciences of the United States of America* 119, no. 22 (2022): e2203680119.

76. A. J. McDonald, "Functional Neuroanatomy of the Basolateral Amygdala: Neurons, Neurotransmitters, and Circuits," *Handbook of Behavioral Neuroscience* 26 (2020): 1–38.

77. N. J. Diederich, G. Stebbins, C. Schiltz, and C. G. Goetz, "Are Patients with Parkinson's Disease Blind to Blindsight?," *Brain* 137, no. Pt 6 (2014): 1838–1849.

Supporting Information

Additional supporting information can be found online in the Supporting Information section.